IOP Publishing Journal of Physics D: Applied Physics
J. Phys. D: Appl. Phys. **56** (2023) 044006 (8pp) https://doi.org/10.1088/1361-6463/acaa44

Multifunctional acoustic metamaterial for air ventilation, broadband sound insulation and switchable transmission

Zhenqian Xiao[1], Penglin Gao[2,3,*], Xiao He[4], Yegao Qu[2,3] and Linzhi Wu[1,4,*]

[1] Center for Composite Materials, Harbin Institute of Technology, Harbin 150001, People's Republic of China
[2] State Key Laboratory of Mechanical System and Vibration, School of Mechanical Engineering, Shanghai Jiao Tong University, Shanghai 200240, People's Republic of China
[3] Institute of Vibration, Shock and Noise, Shanghai Jiao Tong University, Shanghai 200240, People's Republic of China
[4] Key Laboratory of Advanced Ship Materials and Mechanics, College of Aerospace and Civil Engineering, Harbin Engineering University, Harbin 150001, People's Republic of China

E-mail: gaopl@sjtu.edu.cn and wlz@hit.edu.cn

Received 16 October 2022, revised 19 November 2022
Accepted for publication 9 December 2022
Published 22 December 2022

Abstract

Noise reduction and other manipulation of sound waves has been a major concern in science and engineering. Here, we propose a ventilated soundproof acoustic metamaterial consisting of resonant cavities arranged around a central air passage. This metamaterial can accomplish strong sound insulation performance. The transmission loss is larger than 30 dB within a wide frequency range (625–1695 Hz) due to the prohibited band. More intriguingly, we discover that rotating the opening, somewhat like an acoustic switch, can directly control the sound transmission of the deaf band. This is particularly useful for opening a narrow but high transmission window at the frequency of interest, which provides a new degree of freedom for sound control. Through band structure analysis and effective parameter calculation, we discover the sound insulation mechanism of the ventilated metamaterial and reveal the underlying mechanism of the switchable narrow-band sound transmission. Beyond the 1D study, the proposed acoustic metamaterial is expanded to a 3D soundproof metacage. We find that the sound insulation performance and switchable sound transmission phenomena are still retained for the metacage. The results reported here may inspire more exploration of sound barriers and multifunctional applications, such as innovative building facades for noise reduction and logic components for acoustic circuits.

Keywords: acoustic metamaterials, broadband sound insulation, ventilated metastructures

(Some figures may appear in colour only in the online journal)

1. Introduction

Noise pollution is becoming more and more prevalent nowadays and is having an adverse impact on our daily life [1, 2]. Currently, the most popular technique for attenuating airborne sound waves is to install sound barriers, such as walls and micro-perforated panels [3–5], which either absorb or reflect sound waves. Although this method can achieve broadband noise reduction in the medium-to-high-frequency range, due to the limitation of the mass law, heavy and thick barriers are required to increase the sound transmission loss (STL) or broaden the insulation band to the low-frequency range. Alternatively, the use of acoustic elements, such as

* Authors to whom any correspondence should be addressed.

micro-perforated panels with back cavities [6], can also somewhat enhance the sound insulation performance at low frequencies. It is worth noting that these structures hardly allow any airflow through them. However, for air ventilation and heat transfer requirements, which frequently occur in practical applications, a certain amount of airflow has to be allowed. In these circumstances, the applicability of the above structures is undoubtedly very limited. Therefore, there is an urgent need for ventilated sound barriers suitable for low-frequency and broadband applications.

In recent decades, acoustic metamaterial science has fuelled intense interest in noise and vibration engineering, offering a wealth of new designs and insights. In particular, the local resonance mechanism has revolutionized the manipulation of low-frequency waves, producing effective solutions in the fields of noise and vibration reduction [7–10]. It has been particularly successful in reducing sample sizes to deep subwavelength scales [11]; typical examples include, but are not limited to Helmholtz resonators [12–15], labyrinth-type resonators [16–18] and mass-decorated membrane/plate resonators [19–22]. The local resonance essentially increases the scattering and trapping of sound waves and therefore enhances the reflection and absorption effects, which is favorable for sound insulation and absorption applications. Despite the tremendous accomplishments, most of these schemes have the drawback of airflow blockage, which will cause problems in some specific scenarios that require natural ventilation or heat convection. It may seem counterintuitive to reduce noise without obstructing airflow. Therefore, early research on ventilation and noise reduction was very limited in a few industries, for instance, building, where monotonous facade systems such as double-leaf facades and louvers were designed [23, 24]. Some recent developments provide a new perspective on the capacity of ventilated metamaterial for unconventional wave control. Various ventilated acoustic systems have been designed based on the unconventional reflection/absorption mechanism of metamaterial and the theory of duct acoustics. These systems typically involve assembling Helmholtz resonators or labyrinth structures on the ventilation ducts [25–28], as well as some special structures, such as microporous cylindrical shells [29] and ultra-sparse metasurfaces made of Mie resonators [30]. For these systems, a main characteristic is that they have elaborately designed sub-wavelength structures allowing airflow to pass through, but they exhibit very strong blocking of sound waves at certain frequencies. Every coin has two sides: the sound insulation performance of metamaterial is indeed improved, but is at the cost of structural complexity and heaviness, which is undesirable in engineering. In addition, they are designed for a single functionality, achieving either extremely high ventilation ratio or low-frequency sound insulation, but still suffer from weaknesses such as low STL, narrow bandwidth and relatively simple functionality.

Expanding multifunctional applications is a never-ending goal in noise control engineering that is just as significant as reducing structural complexity and broadening sound insulation bands. The sub-wavelength structural details of acoustic metamaterial can provide some unconventional properties not present in natural material, improving its ability to control sound waves. Special phenomena that have the potential for multifunctional applications have been demonstrated, including wavefront modulation [31], sub-diffraction imaging [32] and acoustic cloaking [33]. Zhu [34] designed an acoustic switch with the so-called superfluid phononic crystal that consists of a fluid matrix and fluid-like inclusions with extreme material properties. By rotating the crystal, the band structure can be tuned to obtain an absolute band gap. Babaee *et al* [35] proposed a system comprising an array of elastomeric helices in air and found that its band gap can be suppressed, by stretching the helices, allowing sound to propagate. Ge *et al* [36] designed a metasurface consisting of a series of hook-like meta-atoms whose sound insulation can be switched 'on' or 'off' by adjusting the distance between the two adjacent metasurfaces. However, all these works are limited to special functionalities, not combined with functionalities generally required in life, such as noise reduction and ventilation.

In this study, a well-designed sound barrier that has a relatively simple ventilated structure but achieves strong and broadband sound insulation is reported. We investigate how the ventilation opening affects the sound transmission of the structure and discover that a high transmission window can be opened in the sound insulation band by changing the inclination angle of the opening. To the best of our knowledge, the targeting of multifunctional sound control has not been reported elsewhere. We show that its physical mechanism is related to the so-called 'deaf band' that can be excited or not by modifying the ventilation openings. By changing the geometry of the opening, we can tune the bandwidth of the transmission window. Finally, a ventilated metacage composed of the aforementioned structures is designed that demonstrates the effectiveness of sound insulation and switching functionalities even under 3D conditions. Beyond noise control, the results reported may open new avenues for some fascinating multifunctional applications, such as logic components for acoustic circuits and innovative ventilated building facades.

2. Results and discussion

2.1. Broadband sound insulation

Figures 1(a) and (b) show a sound insulation metamaterial of ventilation holes, which is composed of a number of periodically arranged resonant cavities in series. Each unit has a star-shaped opening in the middle to facilitate free airflow, and the same geometry of side length L and depth d. The star-shaped opening is bordered by four elliptic curves whose major and minor semi-axis lengths are $a = 62$ mm and $b = 31$ mm, respectively. Meanwhile, the sharp corners are rounded with a radius of 0.5 mm. The inclination angle between the long axis of the opening and the horizontal line is θ, which will be discussed in detail later. As shown in figure 1(c), numerical results demonstrate that the designed structure enables

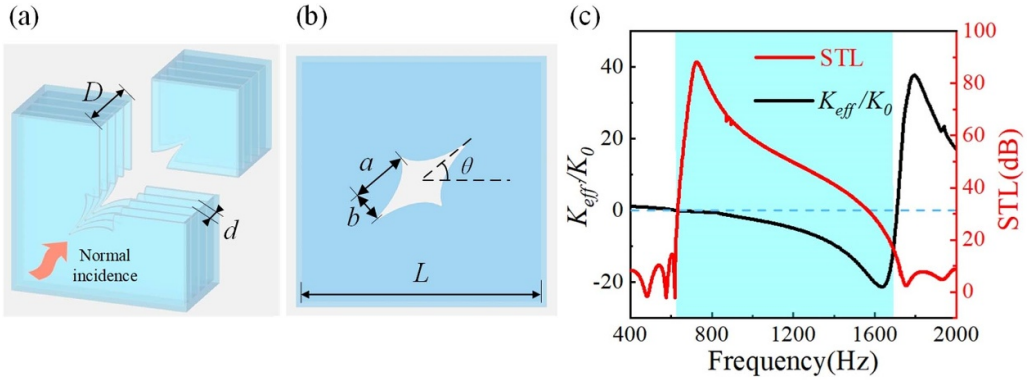

Figure 1. Ventilated metamaterial for broadband sound insulation under normal incidence. Schematic diagram of the sample shown in the (a) section view and (b) front view. (c) Retrieved effective bulk modulus K_{eff}/K_0 and STL of the metamaterial when the inclination angle $\theta = 0°$. Cyan background color borders the sound insulation region, while the dashed horizontal line indicates the critical point of zero effective bulk modulus. Parameters of the sample are defined as follows: total thickness $D = 105$ mm, cavity thickness $d = 20$ mm and side length $L = 200$ mm.

a 30 dB noise reduction in a wide frequency range from 625–1695 Hz.

To uncover the sound insulation mechanism, we first analyze it from the perspective of effective parameters. If an isotropic and homogeneous material can exhibit the same acoustic response as a metamaterial with deep subwavelength structures, it is reasonable to consider the two to be equivalent, i.e. having same material parameters [37]. With this assumption, the effective parameters of the acoustic metamaterial can be obtained by a standard retrieval method and the normalized impedance ξ and effective refractive index n_{eff} of the material can be calculated as [37],

$$\xi = \frac{r}{1-2R+R^2-T^2}, \quad n_{\text{eff}} = \frac{-i\log x + 2\pi m}{kd}, \tag{1}$$

where

$$r = \mp\sqrt{(R^2-T^2-1)^2-4T^2}, \quad x = \frac{1-R^2+T^2+r}{2T}. \tag{2}$$

The sign of r is determined based on the positive acoustic resistance of the passive acoustic metamaterial. The branching number m is assumed to be zero, which corresponds to the minimum thickness of the metamaterial. R and T denote the reflection and transmission coefficients, respectively. The relationship between effective bulk modulus K_{eff}, effective density ρ_{eff}, effective refractive index n_{eff} and effective acoustic impedance Z_{eff} is defined as follows:

$$Z_{\text{eff}} = \frac{\omega\rho_{\text{eff}}}{K_Z}, \quad n_{\text{eff}}^2 = \frac{\rho_{\text{eff}}K_0}{\rho_0 K_{\text{eff}}}, \tag{3}$$

where ω is the angular frequency, and K_0 and ρ_0 are the modulus and density of air, respectively. Moreover, we have quantities ${K_Z}^2 = (\omega/c)^2{n_{\text{eff}}}^2$ and $\xi = Z_{\text{eff}}/\rho_0 c$ with c being the sound velocity in air. The normalized effective density and bulk modulus can be easily obtained:

$$\frac{\rho_{\text{eff}}}{\rho_0} = \xi n_{\text{eff}}, \quad \frac{K_{\text{eff}}}{K_0} = \frac{\xi}{n_{\text{eff}}}. \tag{4}$$

The reflection coefficient, transmission coefficient and STL (STL $= 10\log_{10}|P_{\text{in}}/P_{\text{t}}|$) are calculated in the Pressure Acoustics module of the commercial finite element software COMSOL Multiphysics. By simulating impedance tubes, plane waves are incident normal to the front surface of the metamaterial. Both ends are covered with perfectly matched layers to avoid interference of reflected waves. Due to the large impedance mismatch, the vibroacoustic coupling between thin walls and acoustic waves can be neglected. The visco-thermal effect is not considered here because of the relatively large geometric scales of the cavity and duct. The calculated effective bulk modulus and STL are plotted in figure 1(c), which shows a very strong sound insulation performance with the highest STL up to 90 dB in a broad frequency range from 625–1695 Hz where negative bulk modulus appears. The negative bulk modulus gives rise to an imaginary phase velocity so that no traveling waves can pass through the metamaterial. The broadband sound insulation is essentially caused by the local resonance of the resonators, on the one hand, and the interaction of periodically arranged scatterers, on the other hand, i.e. the locally resonant band gaps and Bragg band gaps. Additional layers can be cascaded in the direction of the wave propagation to further enhance the sound attenuation, but this will increase the sample size. Therefore, we have selected four layers, which is enough to obtain broadband strong sound insulation without making too large-sized structures.

2.2. Switchable sound transmission

Beyond broadband sound insulation, by changing the inclination angle of the opening, the proposed metamaterial can also achieve more intriguing functionality, such as switchable sound transmission. As shown in figure 2, an interesting phenomenon occurs when the opening is rotated 45°. What clearly stands out is a high transmission window between 1210 and 1225 Hz, appearing in the low-transmission sound insulation band. Beyond that, the main features within the sound insulation region remain the same, which suggests that the effective bulk modulus of the metamaterial remains negative. We

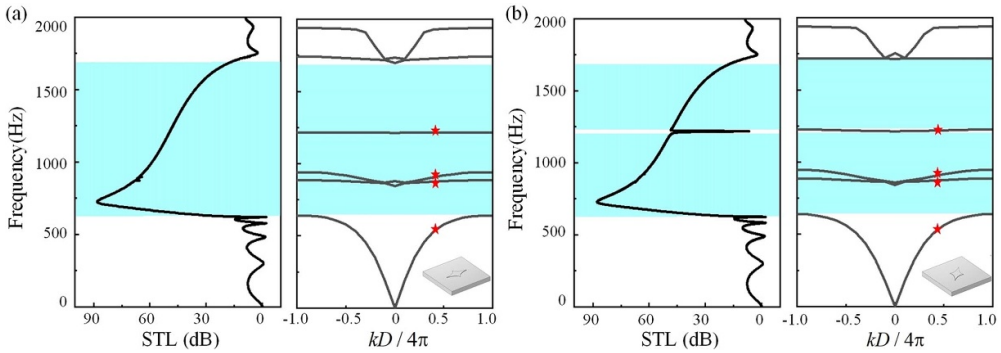

Figure 2. Ventilated metamaterial for switchable sound transmission. Calculated band diagram and STL spectrum when (a) $\theta = 0^\circ$ and (b) $\theta = 45^\circ$, where the cyan-shaded background indicates the sound insulation region. Red stars indicate the eigenmodes illustrated in figure 3. Insets illustrate the unit cells used for the band diagram computation.

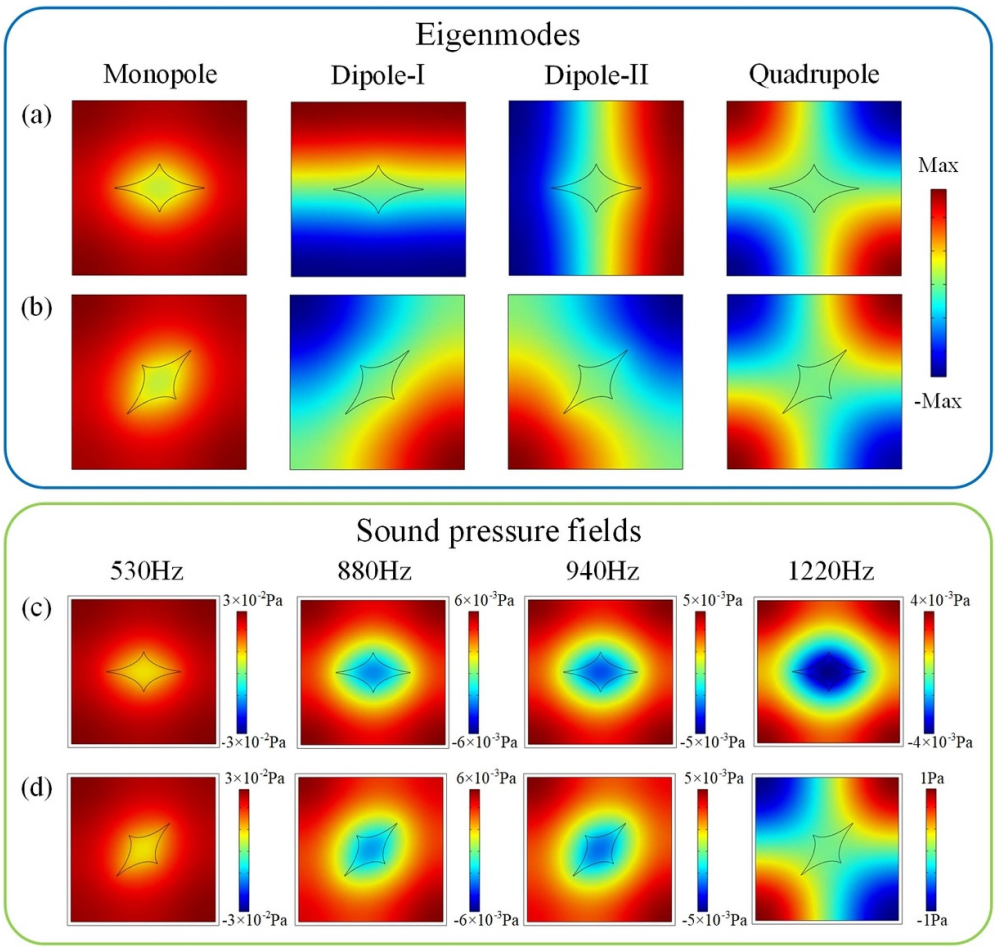

Figure 3. Comparison between the eigenmodes and the excited sound fields. (a), (c) Acoustic eigenmodes and the calculated sound pressure fields for the ventilated metamaterial with $\theta = 0^\circ$. From left to right, the frequency changes as marked in figure 2(a). Likewise, (b) and (d) show the results for the other metamaterial with $\theta = 45^\circ$.

calculate the band diagrams to reveal their transmission properties. The range of the main sound insulation region and the interval between the first five bands are almost perfectly matched, but there are three flat bands appearing in this apparent stopband. Meanwhile, we observe a slight difference between the fourth bands of the two band diagrams shown in figures 2(a) and (b). The one in the left panel is flat, while the other on the right is more disperse. The STL spectrum implies that the three flat bands in figure 2(a) are deaf bands that cannot be excited by the incoming plane waves, while the fourth band in figure 2(b) can be excited by changing the inclination angle of the openings.

In order to have a better understanding, a comparison between the eigenmodes and the excited sound fields is displayed in figure 3 for the two metamaterials previously studied. The sound pressure fields are calculated exactly at

their corresponding eigenfrequencies as marked in figure 2. For the eigenmodes, we see that the monopole, dipole-I and dipole-II modes change with the rotation of the opening, while the quadrupole mode does not. In the first band, the sound pressure fields match well with their eigenmodes, which also happens in the fourth band when $\theta = 45°$, but does not for the other scenarios. The obvious discrepancy indicates that some eigenmodes in the flat bands are not excited by the plane waves. As a result, these bands, which ought to be passbands send up deaf bands instead. This is due to the fact that sound waves can only enter from the opening and spread all the way inside the cavity when the plane wave reaches the structure surface. Therefore, the eigenmodes whose openings do not have plane wavefronts cannot be excited. With this in mind, it is impossible to satisfy the requirement of opposite phases on both sides of the opening of the dipole modes because of the phase mismatch. For the fourth band, it can be explained that when $\theta = 45°$ the wavefront formed in the cavity matches the quadrupole mode exactly, the incident wave can couple with the mode at this time, making it a passband. In contrast, the excitation condition of the quadrupole mode is not satisfied when the opening is positioned at $\theta = 0°$, giving rise to a deaf band. In short, the results show how the excitation conditions of the eigenmodes can be controlled by the inclination angle of the opening, making the soundproof metamaterial act as a sound switch simultaneously.

2.3. *Parametric study on switchable transmission*

In figure 4, we reveal the evolution process of the transmission window opened at 1220 Hz. More specifically, it is found that the high transmission window is not opened immediately at $\theta = 45°$ but rather develops gradually with the increase in θ to the maximum state at $\theta = 45°$. This evolution process comprehensively reflects how the coupling strength between the incident wave and the mode changes from weak to strong. When θ is very small, for example, a few degrees, the coupling to the quadrupole mode is very weak, which means that the quadrupole mode is hardly stimulated so that the transmitted wave is too weak to be observed. In contrast, the passband effect is clearly observed at $\theta = 45°$ because the wave front matches well with the quadrupole mode at this time, resulting in the strongest coupling between the incident wave and the quadrupole mode.

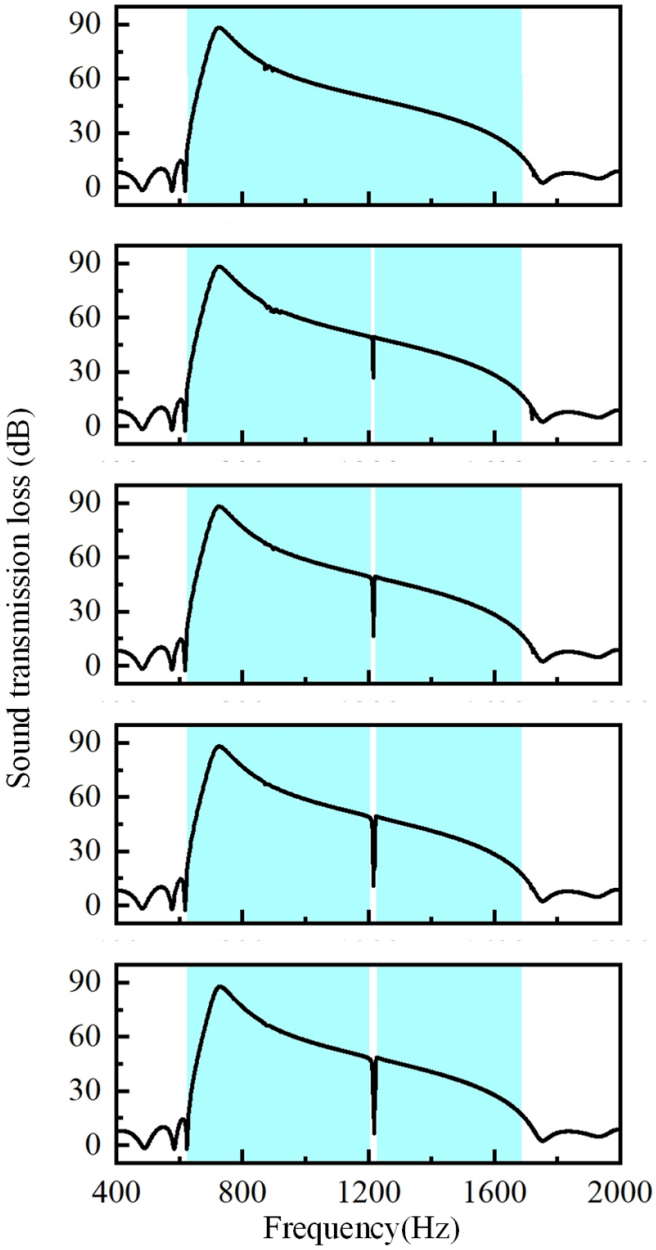

Figure 4. Evolution process of the high-transmission window at 1220 Hz. From top to bottom, the inclination angle θ varies from 0, 11.25°, 22.5°, 33.75° to 45° accordingly.

In figure 5, we investigate the influence of the geometry of the opening on the STL. The minor semi-axis length is maintained as $b = 31$ mm, after which we modify the aspect ratio a/b of the ventilation opening. It is shown that the passband widens as the aspect ratio increases. The reason still lies in the fact that the coupling strength between the eigenmodes and the incident plane waves is different. The larger the aspect ratio, the stronger the coupling. To put it another way, sound waves will propagate to the positive phase region more quickly than to the negative phase region if the opening is longer and narrower, which will result in greater phase difference and stronger coupling with the quadrupole mode. As a result, the quadrupole mode can be excited more easily, leading to high sound transmission. Another phenomenon that can be seen from figure 5 is that the rise frequency of the structure moves to a high frequency as the aspect ratio increases. This is understandable if we note that as the opening area grows with the aspect ratio, more sound waves can propagate through the metamaterial at low frequencies.

In order to further explore the influence of opening shapes on the sound transmission, we consider three ventilation openings of different shapes (ellipse, rhombus and star) while maintaining the same opening area. The star-shaped opening has parameters $a/b = 2$ and $\theta = 45°$, and all other parameters are the same as stated in the caption of figure 1. Although some slight differences are noted, figure 6 illustrates

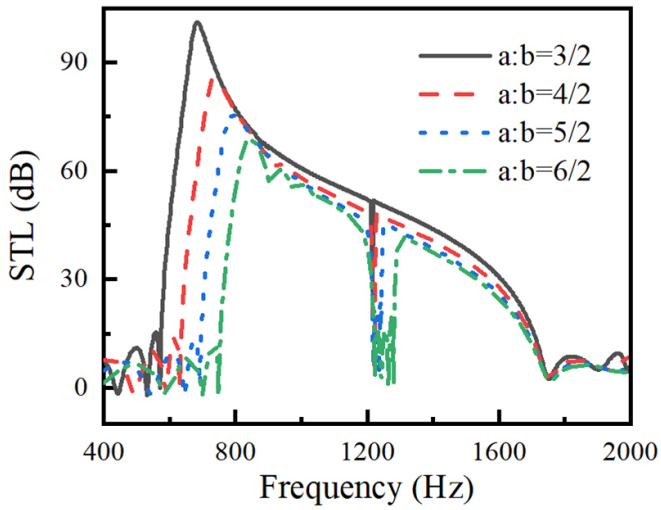

Figure 5. Influence of the aspect ratio a/b of the star-shaped opening on the STL when the inclination angle $\theta = 45°$.

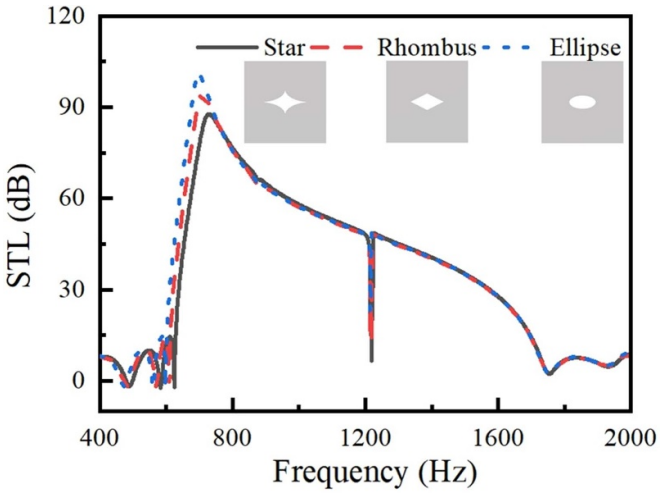

Figure 6. Influence of the geometric shape of the openings on the sound transmission loss.

that the overall sound insulation performance is insensitive to the shape of the openings. However, the geometric shape does affect the transmission windows at 1220 Hz; the star-shaped opening has the highest transmission, followed by the rhombus, and the ellipse is the lowest. As before, the plane wave at the star-shaped opening is more likely to excite the quadrupole mode than the ellipse- and the rhombus-shaped openings. It is worth noting that any ventilation openings of biaxial symmetry have the ability to open the transmission window.

Finally, we design a metacage to demonstrate the acoustic behavior of the 3D structure formed by the aforementioned metamaterial. Figure 7(a) displays a 3D schematic diagram of the computation model. The calculation is implemented in the pressure acoustics module of COMSOL Multiphysics. The 3D acoustic metacage is a cuboid whose six faces are made of the ventilated metamaterial previously studied. Only one unit-cell is used in each facet to save the computational cost, and the faces are connected to each other by rounded corners. Perfectly matched layers are placed around the entire model (parts of the perfectly matched layers are hidden to clearly show the 3D metacage) to reduce unwanted reflections. A loudspeaker that emits spherical waves is placed 500 mm in front of the metacage, and the measurement point is located at the center of the metacage. We calculate the sound pressure levels at the measurement points for two scenarios with and without the metacage, and then measure their difference, i.e. $\Delta_{\mathrm{SPL}} = \mathrm{SPL}_{\mathrm{without}} - \mathrm{SPL}_{\mathrm{metacage}}$, to characterize the sound insulation performance of the 3D metacage. The calculated results presented in figure 7(b) demonstrate that, even under 3D conditions, this metacage is still capable of insulating noise, with a noise reduction of more than 60 dB in the frequency range from 650–1410 Hz. It is no surprise to see a negative value of Δ_{SPL} around 1800 Hz that corresponds to a local enhancement of the acoustic energy outside the band gap. On the other hand, it is worth noting that the phenomenon

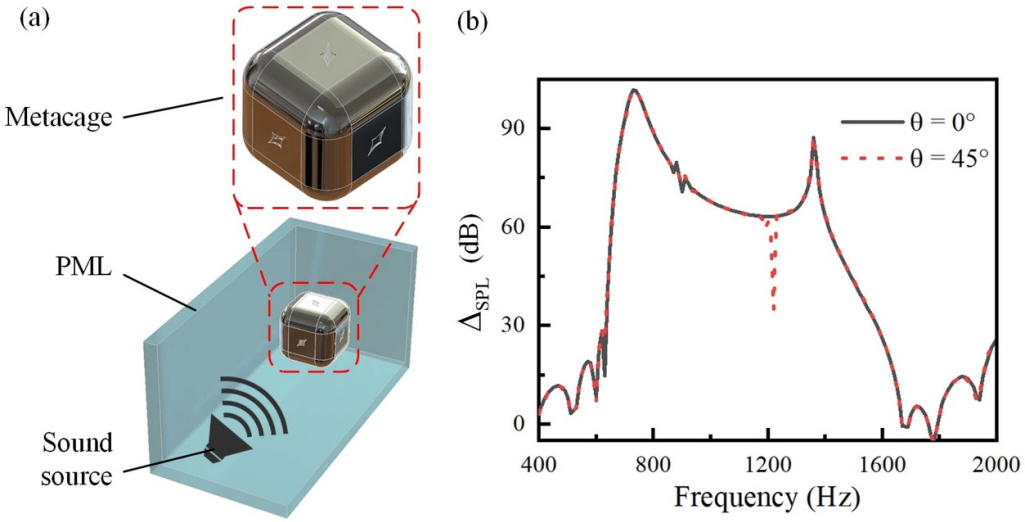

Figure 7. 3D soundproof metacage: (a) schematic diagram of the 3D computation model and (b) the calculated results for sound insulation. Black and red lines represent the cases when $\theta = 0^\circ$ and $\theta = 45^\circ$, respectively.

of the transmission window can still be observed by changing the inclination angle of the opening. This is because the wave striking the metacage can be approximated as a plane wave and thus can couple with the eigenmodes in the fourth band.

3. Conclusion

In this paper, we have designed a kind of ventilated metamaterial for broadband sound insulation and switchable transmission. The metamaterial unit cell consists of an open duct of a resonant cavity. A soundproof system is created by connecting multiple cells in series, with the aim of simultaneously offering ventilation and sound insulation within a specified frequency range. Meanwhile, by changing the inclination angle of the ventilation opening, a straightforward method is proposed to achieve additional functionality of switchable sound transmission. A standard retrieval method has been used to analyze the properties of the metamaterial, revealing a negative material property in its effective bulk modulus. The existence of the deaf band in the sound insulation band is proved through band structure and modal analysis. We show how to convert the deaf band to a passband by adjusting the inclination angle of the opening, which provides a new degree of freedom for sound wave control. Finally, we design a 3D metacage and demonstrate that it still maintains broadband and high sound insulation performance in 3D space. Moreover, the switchable sound transmission phenomenon is still retained. The results here reported may inspire some intriguing applications, such as signal filtering, acoustic communication, acoustic circuits and innovative building facades for multifunctional sound control.

Data availability statement

The data that support the findings of this study are available upon reasonable request from the authors.

Acknowledgments

L W acknowledges the support from the National Natural Science Foundation of China (Grant No. 11702069). Y Q acknowledges the support from the National Natural Science Foundation of China (Grant Nos. U2141244, 11922208, 11932011 and 12121002) and the Oceanic Interdisciplinary Program of Shanghai Jiao Tong University (Grant No. SL2021ZD104). P G acknowledges the support from the National Natural Science Foundation of China (Grant No. 12202267), the Shanghai Pujiang Program (Grant No. 22PJ1405300), the Young Talent Reservoir of CSTAM (Grant No. CSTAM2022-XSC-QN1) and the Starting Grant of Shanghai Jiao Tong University (Grant No. WH220402014).

Conflict of interest

The authors declare that they have no known competing financial interests or personal relationships that could have appeared to influence the work reported in this paper.

ORCID iD

Penglin Gao https://orcid.org/0000-0002-8473-2844

References

[1] Bies D A, Hansen C H and Howard C Q 2017 *Engineering Noise Control* (Boca Raton, FL: CRC Press)
[2] Qu S, Gao N, Tinel A, Morvan B, Romero-García V, Groby J P and Sheng P 2022 Underwater metamaterial absorber with impedance-matched composite *Sci. Adv.* **8** eabm4206
[3] Zhang Z M and Gu X T 1998 The theoretical and application study on a double layer microperforated sound absorption structure *J. Sound Vib.* **215** 399–405
[4] Wang C and Huang L 2011 On the acoustic properties of parallel arrangement of multiple micro-perforated panel

absorbers with different cavity depths *J. Acoust. Soc. Am.* **130** 208–18
[5] Guillen I, Uris A, Estelles H, Llinares J and Llopis A 2008 On the sound insulation of masonry wall façades *Build. Environ.* **43** 523–9
[6] Park S H 2013 Acoustic properties of micro-perforated panel absorbers backed by Helmholtz resonators for the improvement of low-frequency sound absorption *J. Sound Vib.* **332** 4895–911
[7] Gao P, Sánchez-Dehesa J and Wu L 2018 Poisson-like effect for flexural waves in periodically perforated thin plates *J. Acoust. Soc. Am.* **144** 1053–8
[8] Wang Y F, Wang Y Z, Wu B, Chen W Q and Wang Y S 2020 Tunable and active phononic crystals and metamaterials *Appl. Mech. Rev.* **72** 040801
[9] Gao P, Climente A, Sánchez-Dehesa J and Wu L 2019 Single-phase metamaterial plates for broadband vibration suppression at low frequencies *J. Sound Vib.* **444** 108–26
[10] Gao P, Zhang Z and Christensen J 2020 Sonic valley-Chern insulators *Phys. Rev.* B **101** 020301
[11] Ma G and Sheng P 2016 Acoustic metamaterials: from local resonances to broad horizons *Sci. Adv.* **2** e1501595
[12] Cai X, Guo Q, Hu G and Yang J 2014 Ultrathin low-frequency sound absorbing panels based on coplanar spiral tubes or coplanar Helmholtz resonators *Appl. Phys. Lett.* **105** 121901
[13] Huang S, Fang X, Wang X, Assouar B, Cheng Q and Li Y 2019 Acoustic perfect absorbers via Helmholtz resonators with embedded apertures *J. Acoust. Soc. Am.* **145** 254–62
[14] Guo J, Zhang X, Fang Y and Jiang Z 2020 A compact low-frequency sound-absorbing metasurface constructed by resonator with embedded spiral neck *Appl. Phys. Lett.* **117** 221902
[15] Tang Y, He W, Xin F and Lu T J 2020 Nonlinear sound absorption of ultralight hybrid-cored sandwich panels *Mech. Syst. Signal Process.* **135** 106428
[16] Frenzel T, David Brehm J, Bückmann T, Schittny R, Kadic M and Wegener M 2013 Three-dimensional labyrinthine acoustic metamaterials *Appl. Phys. Lett.* **103** 061907
[17] Wang Y, Zhao H, Yang H, Zhong J and Wen J 2017 A space-coiled acoustic metamaterial with tunable low-frequency sound absorption *Europhys. Lett.* **120** 54001
[18] Xiao Z, Gao P, Wang D, He X and Wu L 2021 Ventilated metamaterials for broadband sound insulation and tunable transmission at low frequency *Extreme Mech. Lett.* **46** 101348
[19] Mei J, Ma G, Yang M, Yang Z, Wen W and Sheng P 2012 Dark acoustic metamaterials as super absorbers for low-frequency sound *Nat. Commun.* **3** 1–7
[20] Chen Y, Huang G, Zhou X, Hu G and Sun C T 2014 Analytical coupled vibroacoustic modeling of membrane-type acoustic metamaterials: membrane model *J. Acoust. Soc. Am.* **136** 969–79
[21] Huang T Y, Shen C and Jing Y 2016 Membrane-and plate-type acoustic metamaterials *J. Acoust. Soc. Am.* **139** 3240–50
[22] Xu Q, Qiao J, Sun J, Zhang G and Li L 2021 A tunable massless membrane metamaterial for perfect and low-frequency sound absorption *J. Sound Vib.* **493** 115823
[23] Bajraktari E, Lechleitner J and Mahdavi A 2015 The sound insulation of double facades with openings for natural ventilation *Build. Acoust.* **22** 163–76
[24] Zuccherini Martello N, Fausti P, Santoni A and Secchi S 2015 The use of sound absorbing shading systems for the attenuation of noise on building facades. An experimental investigation *Building* **5** 1346–60
[25] Yu X, Lu Z, Cheng L and Cui F 2017 On the sound insulation of acoustic metasurface using a sub-structuring approach *J. Sound Vib.* **401** 190–203
[26] Kumar S, Xiang T B and Lee H P 2018 Ventilated acoustic metamaterial window panels for simultaneous noise shielding and air circulation *Appl. Acoust.* **159** 107088
[27] Yang J, Lee J S, Lee H R, Kang Y J and Kim Y Y 2018 Slow-wave metamaterial open panels for efficient reduction of low-frequency sound transmission *Appl. Phys. Lett.* **112** 091901
[28] Ghaffarivardavagh R, Nikolajczyk J, Anderson S and Zhang X 2019 Ultra-open acoustic metamaterial silencer based on Fano-like interference *Phys. Rev.* B **99** 024302
[29] García-Chocano V M, Cabrera S and Sánchez-Dehesa J 2012 Broadband sound absorption by lattices of microperforated cylindrical shells *Appl. Phys. Lett.* **101** 184101
[30] Cheng Y, Zhou C, Yuan B G, Wu D J, Wei Q and Liu X J 2015 Ultra-sparse metasurface for high reflection of low-frequency sound based on artificial Mie resonances *Nat. Mater.* **14** 1013–9
[31] Xie Y, Wang W, Chen H, Konneker A, Popa B I and Cummer S A 2014 Wavefront modulation and subwavelength diffractive acoustics with an acoustic metasurface *Nat. Commun.* **5** 1–5
[32] Smith D R, Schurig D, Rosenbluth M, Schultz S, Ramakrishna S A and Pendry J B 2003 Limitations on subdiffraction imaging with a negative refractive index slab *Appl. Phys. Lett.* **82** 1506–8
[33] Chen Y, Zheng M, Liu X, Bi Y, Sun Z, Xiang P, Yang J and Hu G 2017 Broadband solid cloak for underwater acoustics *Phys. Rev.* B **95** 180104
[34] Zhu X F 2012 Acoustic waves switch based on meta-fluid phononic crystals *J. Appl. Phys.* **112** 044509
[35] Babaee S, Viard N, Wang P, Fang N X and Bertoldi K 2016 Harnessing deformation to switch on and off the propagation of sound *Adv. Mater.* **28** 1631–5
[36] Ge Y, Sun H, Yuan S and Lai Y 2019 Switchable omnidirectional acoustic insulation through open window structures with ultrathin metasurfaces *Phys. Rev. Mater.* **3** 065203
[37] Fokin V, Ambati M, Sun C and Zhang X 2007 Method for retrieving effective properties of locally resonant acoustic metamaterials *Phys. Rev.* B **76** 144302